CORA Cork Open Research Archive
Cartlann Taighde Oscailte Chorcaí

Title	Confined growth and crystallography of one-dimensional Bi2S3, CdS and SnSx nanostructures within chaneled substrates
Authors	Petkov, Nikolay;Xu, Ju;Morris, Michael A.;Holmes, Justin D.
Publication date	2008-04-11
Original Citation	Petkov, N., Xu, J., Morris, M. A. and Holmes, J. D. (2008) 'Confined Growth and Crystallography of One-Dimensional Bi2S3, CdS, and SnSx Nanostructures within Channeled Substrates', The Journal of Physical Chemistry C, 112(19), pp. 7345-7355. doi: 10.1021/jp800193x
Type of publication	Article (peer-reviewed)
Link to publisher's version	https://pubs.acs.org/doi/full/10.1021/jp800193x - 10.1021/jp800193x
Rights	© 2008 American Chemical Society. This document is the Accepted Manuscript version of a Published Work that appeared in final form in The Journal of Physical Chemistry C, copyright © American Chemical Society after peer review and technical editing by the publisher. To access the final edited and published work see https://pubs.acs.org/doi/full/10.1021/jp800193x
Download date	2026-11-02 18:37:45
Item downloaded from	https://hdl.handle.net/10468/8153

UCC
University College Cork, Ireland
Coláiste na hOllscoile Corcaigh

Confined Growth and Crystallography of One-Dimensional Bi_2S_3, CdS and SnS_x Nanostructures within Channeled Substrates

Nikolay Petkov[1,2], Xu Ju[1], Michael A. Morris[1,2] and Justin D. Holmes[1,2]

[1]Department of Chemistry, Materials Section and Supercritical Fluid Centre, University College Cork, Ireland, [2]Centre for Research on Adaptive Nanostructures and Nanodevices (CRANN), Trinity College Dublin, Dublin 2, Ireland.

AUTHOR EMAIL ADDRESS j.holmes@ucc.ie

RECEIVED DATE (to be automatically inserted after your manuscript is accepted if required according to the journal that you are submitting your paper to)

TITLE RUNNING HEAD One dimensional Bi2S3, CdS and SnSx nanostructures, confined within the channels of the anodic alumina membranes.

CORRESPONDING AUTHOR FOOTNOTE: Justin D. Holmes, e-mail: j.holmes@ucc.ie

ABSTRACT The growth, composition and structural properties of one dimensional Bi_2S3, CdS and SnS_x nanostructures, confined within the channels of anodic alumina membranes, have been comprehensively investigated by electron microscopy and spectroscopy. In particular, the morphology, loading factors, crystal structure and orientation and potential growth mechanisms of the II-VI nanostructures confined within the alumina templates, with mean pore diameters of 80 and 20 nm, were investigated. A solventless pressure-injection method was used to form ordered arrays of these 1 D nanostructures, with controlled diameters (by the dimensions of the templating channels), controlled orientations (via the direction of the templating channels) and isolated from each other within the

alumina templates. A variety of 1 D nanostructures ranging from well faceted nanowires to nanotubes and nanobelts have been identified and characterized. For all of the materials investigated, single crystalline and oriented structures were observed having preferred growth directions within the alumina channels.

KEYWORDS Nanowires, anodic alumina, crystallography, confined growth.

BRIEFS The growth, composition and structural properties of one dimensional Bi_2S_3, CdS and SnS_x nanostructures, confined within the channels of the anodic alumina membranes, have been comprehensively investigated by electron microscopy and spectroscopy.

MANUSCRIPT TEXT

Introduction

One-dimensional (1 D) nanostructures are attracting a great deal of attention due to their unique properties and potential novel applications.[1] Template-assisted methods for depositing 1 D nanostructured materials, pioneered by Martin, Searson and Mallouk, have shown appealing possibilities for the confined growth of ordered arrangements of a variety of nanostructures.[2] For example, applying anodic alumina membranes (AAMs) or ordered mesoporous materials (OMMs), ordered arrays of 1 D nanostructures ranging from carbon nanotubes and metal oxides to semiconductors and metals have been obtained.[3] Various approaches, including electrochemical and electroless deposition, sol-gel, paired-cell, chemical vapour deposition, and supercritical fluid deposition have been exploited to deposit a range of 1 D materials with single crystalline, polycrystalline or amorphous structure within these templates.[4] Notably these methods are characterised by specific growth mechanisms and inclusion pathways, ruled by the type of template support and deposition procedure. Recently, we have reported a pressure-injection solventless approach, without the use of a catalyst or complexing agent, to synthesize single crystalline and oriented Bi_2S_3 nanowire arrays within AAMs.[5] Here we present data on the growth and crystal structures of Bi_2S_3, CdS and SnS_x nanostructures prepared by solventless growth within the channels of AAMs.

Among the metal sulfides Bi_2S_3, CdS and SnS_x semiconductors show intriguing thermoelectric, optoelectronic and photovoltaic properties. These properties are manifested in a variety of potential applications such as solar cells, laser diodes, photoconductors, photovoltaic and thermoelectric devices.[6] One-dimensionality in the structure of the Bi_2S_3, CdS and SnS_x materials can additionally diversify their properties especially when the structure of the surfaces starts to dominate their bulk properties. Besides the practical reasons to study 1 D nanostructures of metal sulfides, the fundamental aspects of their structure and morphology in confined environments, such as those within the channels of the AAMs, are of interest. Specifically, characteristics such as crystal structure, morphology, surface states and defects can be considerably altered when nanostructures are prepared within 1 D channel supports.[8]

Electron microscopy has proven to be one of the most powerful tools for characterizing 1 D nanostructures allowing determination of crystal and surface structure, defect sites, grain boundaries and chemical composition.[8] When 1 D nanostructures are prepared within channeled substrates with ordered porosity, electron microscopy, combined with electron diffraction and chemical analysis, can give additional evidence of the encapsulation process, loading factors, number density, spatial distribution and crystal orientation of the deposited materials.

The objective of this paper is to present a comprehensive investigation of the growth process and structure of 1 D Bi_2S_3, CdS and SnS_x nanostructures within the channels of AAMs by electron microscopy and spectroscopy. Important structural and growth characteristics of the metal sulfides within the confining environment of 80 and 20 nm channels are discussed.

Experimental

AAMs with average pore diameters of approximately 80 and 20 nm, prepared by well established literature methods, were used as hard templates for the encapsulation of the 1 D metal sulfides. Arrays of Bi_2S_3, CdS and SnS_x nanostructures were prepared following a solventless pressure–injection technique utilizing single source precursors bis(diethyldithiocarbamate) [$Bi(S_2CNEt_2)_3$], bis(diethyldithiocarbamate) [$Cd(S_2CNEt_2)_2$] and bis(diethyldithiocarbamate) [$Sn(S_2CNEt_2)_2$],

respectively. The precursors have melting points around 200 °C, and a decomposition temperature around 300 °C, which makes them suitable for direct pressure-injection within the AAMs channels. In a typical experiment, the organometallic precursor (~300 mg) was positioned on the outer surface of the AAM template in a sealed glass tube. The tube was then heated to 270 °C under vacuum to melt the precursor and the temperature was maintained for additional 60 min. The decomposition of the precursors was achieved at a constant temperature of 300 °C for 4 h. After the reaction, the reaction cell was cooled to room temperature and the substrates were washed with 10 mL of acetone.

The surface morphology of the samples was determined on a by JEOL, JSM 6500 scanning electron microscopy (SEM) equipped with an Oxford energy dispersive x-ray (EDX) detector. The TEM images were obtained with a JEOL 2010 transmission electron microscope (TEM) operating at 200 kV, equipped with an Oxford EDX detector. Samples for electron microscopy were prepared by the following methods: (i) the alumina matrix was dissolved in phosphoric acid to release the embedded nanostructured materials; (ii) plan-views and cross-sections were prepared by dimple grinding, followed by Ar-ion polishing. The dimple grinding was accomplished using a Gatan dimple grinder Model 656, using 5 μm diamond paste. The precision Ar-ion polishing was done at grazing angles of 6° at a 5 kV acceleration voltage using a Gatan, precision ion polishing system (PIPS), Model 691. XRD measurements were performed with a Philips X'Pert diffractometer using Cu $K\alpha_1$ radiation. The measurements were done in reflection (θ - 2θ) geometry.

Results and Discussion

Morphology, loading factors and composition

Morphology and composition are of primary interest when dealing with the inclusion of different materials within porous templates. It is expected that the shapes and directions of the pores within a porous matrix can guide the type of morphology and orientation of the encapsulated materials. For example, spherically shaped nanopores are used to embed nanosized particles with dimensions corresponding to the diameters of the spherical pores. Similarly, channelled templates (such as AAMs)

are expected to shape the growth of 1 D nanostructures, provided that the growth process is efficient enough to guarantee extended filling of the 1 D porous system. Nevertheless, in many cases the morphology of the encapsulated materials can differ significantly from the shape of the templating nanopores. In these cases electron microscopy is an essential characterisation tool for examining included materials directly within the porous systems. This is even more important when the porous structures are assembled as layers or membranes with specific orientations of the templating nanopores. The observation of encapsulated materials together with the templating matrix can by achieved by SEM or TEM of cross-sectional or plan-view specimens. For example Figure 1 (a) and (b) shows cross-sectional SEM and TEM images of Bi_2S_3 nanowires encapsulated within the vertical channels of AAMs with mean pore diameters of 80 and 20 nm. The brighter segments observed in the SEM image (Figure 1(a)), shown with black arrows, correspond to Bi_2S_3 nanowires with diameters of between 70-80 nm. The darker parts observed in the TEM image (Figure 1(b)), shown by white arrows, are Bi_2S_3 nanowires with diameters between 15-20 nm. The nanowires appear well-structured within the channels and are restricted by the dimensions of the pores, giving ordered arrays of vertically aligned 1 D nanostructures. The shapes and diameters of the 1 D nanostructures correspond to those of the templating channels nevertheless sometimes nanowires with diameters smaller than the membrane channels were also observed. The other possibility of viewing the nanostructures is to image cross-sections of the nanostructures by TEM, with the electron beam oriented parallel to the long axis of the AAMs channels, referred to as plan-view imaging (see Supporting Information). Generally, this type of imaging allows for a larger number of nanostructures to be sampled and analyzed. Thus distributions of nanowire diameters, number density and loading factors can be calculated. For example, the average nanowire diameter and loadings of the Bi_2S_3 nanowires within the 80 and 20 nm AAMs were d = 70 ±10 and 18 ±5 nm; 75 % and 65 %, respectively. Precise observation of the whole length of the nanowires is quite elaborated and normally requires dissolution of the membrane. By examining large numbers of such images, it was confirmed that the Bi_2S_3 nanowires have lengths of about 10 µm, with some nanowires exceeding several tens of micrometers (see Supporting Information).

Similarly, CdS nanostructures were examined. Figure 1 (c) and (d) show examples of such nanostructures liberated from the alumina templates. The diameter of the nanowires is controlled by the diameter of the channels within the AAMs thus producing nanowires with defined diameters. The average nanowire diameter and loading factors of the CdS nanowires within the 80 and 20 nm alumina membranes were: d = 78 ±5 and 20 ±3: 65 % and 60 %, respectively. These numbers were calculated by examining a number of plan-view TEM images (see Supporting Information). These results suggest that lower loadings of CdS nanowires were obtained within the channels of the alumina matrix in comparison to the Bi_2S_3 samples. It can be seen that all of the CdS nanowires are filling the whole interior of the channels within the templates, thus giving a sharper size distribution of nanowire diameters in comparison to the Bi_2S_3 nanowires.

The SnS_x structures within AAMs were investigated likewise and showed a completely different type of 1 D nanostructure. Figures 2 (a) and (b) show that the nanostructures are indeed encapsulated within the 80 and 20 nm channels of the AAMs, but their morphology differs significantly from the shape of the confining channels. Generally nanobelt-like structures were formed having different belt thicknesses; yet nanowire-like structures were also observed. In some cases faceted nanotubes or half-tubes were seen (shown with arrows in Figure 2(a)), formed most probably by confining a nanobelt within a single channel (see below). In order to precisely identify the cross-sectional morphology of the SnS_x nanostructures they were observed in the TEM with the electron beam parallel to the long axis of AAMs channels (Figure 2 (c) and (d)). It is observed that the thickness of the nanobelts within the channels varied between 10-60 nm for the structures deposited in the 80 nm AAMs, and between 5 – 15 nm for the structures deposited within the 20 nm AAMs. The loading factors for the 80 and 20 nm membranes were 50 % and 55 %, respectively. These numbers are lower than the number density and the loading factors calculated for the Bi_2S_3 samples.

The remarkable difference in the morphology of the encapsulated nanostructures within the AAMs channels, obtained by applying similar deposition conditions, can be explained by taking into account

the intrinsic crystalline structure of the deposited materials and their interaction with the walls of the confining alumina channels. Most importantly electron microscopy allows us to observe that by combining the solventless pressure-injection method and AAMs as hard templates, ordered arrays of 1 D nanostructures with controlled diameters (determined by the dimensions of the templating channels), controlled orientations (determined by the orientation of the templating channels) and isolated from each other within an alumina matrix can be formed.

The composition of the deposited materials within the porous templates and their uniformity across the templating matrix is of primary importance when examining the encapsulation of nanostructured materials. Most of the well-known analytical techniques, *e.g.* mass-spectrometry ICP, XRF, XPS etc are of limited use for examining encapsulated materials because of their inability to differentiate between materials embedded within a templating matrix and these are deposited on the outer surface. For example, the deposition of nanomaterials within the channels of AAMs, by a variety of techniques that include sol-gel, chemical vapour deposition, electroless, supercritical fluid deposition, usually results in large amounts of material being formed on the outer surface of the membranes. The composition and structure of this surface material may differ significantly from the material deposited within the pores. In this case microanalysis, using energy dispersive X-ray (EDX) spectroscopy is of primary importance. Cross-sectional samples of Bi_2S_3, SnS_x and CdS templated within 80 nm alumina membranes were investigated in this way. Figures 3 (a) and (b) show cross-sectional SEM images together with EDX spectra, taken from top to bottom of the membrane, of an alumina template incorporated with Bi_2S_3 nanowires. By quantifying the EDX spectra obtained along the length of the membrane, it was confirmed that the deposited material is indeed Bi_2S_3 (Bi/S atomic ratios of 0.64 – 0.67) across the entire membrane thickness. At the same time it was verified that the loading is not uniform across the length of the channels within the membrane. The loading is almost 100 % close to one of the membrane surfaces; for example spec 7 on Figure 3 (a) shows a Bi/Al weight ratio of 1.35 which is very close to the calculated maximum loading ratio for Bi/Al of 1.4. The loading decreases to about 15 % at the other membrane surface, see for example spec 1 with a Bi/Al weight ratio of 0.2. Similarly, the EDX analysis

of the membranes containing CdS nanostructures confirmed the existence of CdS (Cd/S atomic ratios of 0.98-1.02) and non-uniform filling of the channels ranging between 10-90 % across the thickness of the membrane (Figure 3 (c)). EDX analysis of the SnS_x nanostructures across the length of the channels in the alumina membranes resulted in Sn/S atomic ratios between 0.58 – 0.74, suggesting mixed SnS and SnS_2 stoichiometries of the deposited materials. The nanostructures showed higher loadings of about 60 % at one end of the membrane surface, reducing to 17 % at the other end (Figure 3 (d)). Similar investigations were performed on cross-sectional samples of Bi_2S_3, CdS and SnS_x nanostructures within 20 nm AAMs and similar loading factors as these for the 80 nm membranes, with pronounced non-uniform loading of nanostructures within the channels of the membrane, were obtained.

When comparing the loading factors obtained by EDX analysis and those calculated by observing plan-view TEM images, one should take into account that the plan-view TEM imaging was conducted over thin specimens extracted from the middle of the membranes. In this way, spec 5 from the Bi_2S_3 sample taken from the middle of the membrane (Figure 3 (a)) and showing a loading of approximately 75 % is very similar to the loadings calculated from the plan-view TEM images. In general, EDX measurements across the membrane thickness should be considered more appropriate for determining the loading factors within the membranes since they take into account larger excitation volumes than the areas observed by the TEM images. Furthermore, cross-sectional EDX measurements are critical when examining the distribution of loadings across the membrane thickness.

Crystal structure, growth directions and defects

Electron microscopy and diffraction gives a unique opportunity to investigate the crystal structure and orientation of nano-sized materials. Here we use HRTEM combined with small-area electron diffraction (SAED) to examine the crystal structure, orientation and possible defects of Bi_2S_3, SnS_x and CdS nanostructures both within the channels of AAMs and liberated form the alumina matrix. *Crystal Structure* software package was used to simulate electron diffraction patterns by using appropriate lattice cell dimensions and help to identify and index the obtained SAED patterns. For comparison X-ray diffraction analysis of as-synthesized and polished composite membranes was also conducted.

Figure 4 (a) shows XRD patterns of as-deposited and polished alumina membranes containing Bi_2S_3 nanowires. The as-deposited specimens showed a number of reflections that can be indexed to the orthorhombic bismuthinite structure (reference pattern, JCPDS No. 170320). The XRD patterns from the polished 80 and 20 nm membranes display one high intensity reflection emanating from the {002} set of planes, at 48.2 2θ degrees, indicating that the Bi_2S_3 nanowires have preferential orientation along the [002] direction. This remarkable difference in the XRD characteristics of the Bi_2S_3 crystals on the surface *vs* the polished samples can be explained by the fact that in the reflection XRD experiment (θ - 2θ) only the crystallographic planes parallel to the sample surface can be detected. Thus randomly oriented Bi_2S_3 crystals on the membrane surface give rise to powder-like patterns whereas the preferentially oriented nanowires inside the channels of the AAMs results in a reduced number of reflections, corresponding to planes parallel to the membrane surface, *i.e.* the (002) reflection.

Figure 5 shows TEM images of 80 and 20 nm Bi_2S_3 nanowires, isolated from both types of membranes, respectively. Bright-field imaging of the wires revealed variations in the contrast due to the thickness fringes, well-known phenomenon observed when imaging single crystal nanowires. To understand the thickness fringes, the two-beam diffraction conditions should be considered, one is the transmitted beam, and the other is the diffracted beam. Briefly, an increase in crystal thickness results in an oscillation of the diffracted beam due to the multiple-scattering effects, producing the thickness fringes. The corresponding change in crystal thickness for two adjacent thickness fringes can be a few nanometers. The SAED patterns of the two nanowires shown on Figure 5 (c) and (d) verify their single crystalline nature indicated by sharp diffraction dots. The indexation of the SAED patterns was done by first simulating the patterns by using appropriate lattice cell dimensions for orthorhombic *Pbnm* space group (a = 1.114 nm; b = 1.113 nm; c = 0.398 nm), and corresponding Bi and S atomic coordinates, followed by fitting the simulations to the recorded SAED data. Thus it was determined that the SAED patterns were taken with the electron beam along the [010] direction and that the nanowires were grown along the [002] direction. Additionally, HRTEM imaging was undertaken to directly visualize the crystal structure and determine the growth direction. Figure 5 (f) provides evidenced for the single

crystalline nature of a 20 nm nanowire with clearly visible lattice fringes. The lattice fringes with a d-spacing of about 0.37 nm, attributed to the (101) lattice planes, are observed. Fast Fourier transformation (FFT) of this HRTEM image (inset in Figure 5 (f)) allows for accurate determination of the d-spacing values and further validate the [002] direction as the growth direction of the nanowires, with the {101}, {301} and {200} lattice planes oriented at 20, 45 and 90 degrees to the growth direction, respectively. Additionally, by examining a few tens of nanowires by SAED and FFTs of the HRTEM images it was observed that the only growth direction for the 80 and 20 nm nanowires was along the [002] zone axis. All of the nanowires showed no evidence of planar defects (stacking faults, twins or bicrystals) or dislocations and appeared well-faceted and uniform. These data are in good agreement with the obtained XRD results and correspond to other published results for single crystalline Bi_2S_3 nanowires and nanorods grown by template-free methods.

Similarly, CdS nanowires grown within the AAMs were examined and the XRD patterns of the as-synthesized and polished specimens are shown on Figure 4 (b). Unpolished membranes, containing material on the outer surface, showed a number of reflections that can be indexed to the hexagonal cadmium yellow structure (reference pattern, JCPDS No. 06-0314). In comparison, after polishing, both the 80 and 20 nm AAMs showed one highly intensive reflection corresponding to the {002} set of planes, at 26.6 2θ degrees, indicating that the CdS nanowires have a highly preferential orientation along the [002] direction. These results are very similar to the XRD data collected for the Bi_2S_3 nanowires within the AAMs. To further examine the crystal structure and orientation of the CdS nanowires, SAED and HRTEM imaging was undertaken. Figure 6 shows TEM images of two CdS nanowires, grown within 80 and 20 nm alumina templates, and the corresponding SAED patterns obtained from these wires. The CdS nanowires showed less pronounced thickness fringes along their lengths than the Bi_2S_3 samples. The SAED patterns have single crystal like signatures with elliptical diffraction spots (Figure (c) and (d)). This data is indicative of distortion of the single crystal structure in the nanowires due to strain produced by adopting strictly cylindrical shapes in the absence of well-developed facets. The simulation of the SAED is done considering a hexagonal *P63mc* space group with appropriate unit cell

parameters (a = 0.414 nm; b = 0.414 nm; c = 0.672 nm) and atomic positions. Thus it was determined that the SAED patterns were taken with the electron beam parallel to the [100] zone axis, and perpendicular to the [002] direction which is the growth direction of the nanowire (in line with the XRD data). A HRTEM image of a 20 nm CdS nanowire, taken with the electron beam parallel to the alumina channel, is shown in Figure 6 (f). Well-developed crystalline fringes with a d-spacing of 0.35 nm corresponding to the {100} set of planes were observed, perpendicular to the (002) planes in good agreement with the SAED and X-ray diffraction data. These facts illustrate that well crystalline and oriented CdS nanowires are formed by adopting the cylindrical shapes of the templating channels. The nanostructres are filling the whole interior of the AAMs channels and appeared less faceted than the Bi_2S_3 nanowires.

Similarly SnS_x nanostructures, with their complex variety of 1 D shape and morphology, were examined. XRD patterns for the as-deposited and polished membranes are presented on Figure 4 (c). A number of reflections that can be indexed to the orthorhombic herzenbergite SnS structure (reference pattern, JCPDS No. 14-0620, shown with black bars) were recorded for the material, over-grown on the membrane surface. However, the XRD patterns of the polished 80 and 20 nm membranes showed several peaks at 28.1, 30.5, 45.1 and 50.1 2θ degrees, that can not be assigned by assuming that only single phase SnS has been formed. In fact, only the reflections at 30.5 and 45.1 2θ degrees correspond to the {101} and {002} set of planes of the SnS phase. The reflections at 28.1, 30.5 and 50.1 2θ degrees can be indexed as the (110), (011) and (121) reflections of the hexagonal SnS_2 (berndtite) structure (reference pattern, JCPDS No. 21-1231, shown with pink bars). The corresponding directions can be considered as possible preferred growth directions for the encapsulated SnS and SnS_2 nanostructures within the AAMs.

The structural data was further verified by performing SAED on isolated SnS_x nanostructures. For example, Figures 7 (a) and (b) show two nanobelt structures isolated from the 80 templates, and the corresponding SAED patterns. The nanostructures exhibit pronounced thickness fringes and single crystalline diffraction patterns confirming the formation of well crystalline facets. The SAED pattern on

Figure 7 (c) is indexed with the help of a simulated ED pattern (Figure 7 (e)) corresponding to the SnS phase (orthorhombic unit cell *Pnma*, a = 1.118 nm; b = 0.398; c = 0.432 nm) and taken with electron beam along the [010] direction. Thus it was verified that the nanostructure is indeed SnS and is grown along the [002] direction. The other example, shown on Figure 7 (d), is of the SnS_2 phase (hexagonal unit cell *P63mc*, a = 0.365 nm; b = 0.365 nm; c = 0.58992 nm) and is grown along the [121] direction, determined based on the SAED pattern (Figure 7 (f)), simulated with the electron beam along the [111] direction. The corresponding growth directions are in a good agreement with the XRD data, showing co-existence of SnS and SnS_2 phases within the channels with several different growth directions, being [002] for the SnS phase and [121] for the SnS_2 phase. The other possible growth directions, *e.g.* [101] for the SnS phase, and [110] or [011] for the SnS_2 phase were also observed (Figure 8 and Supporting Information) in specimens isolated from 80 and 20 nm membranes, and verified by measured and simulated SAED patterns. Generally, nanobelts, as opposed to nanowires, can be considered as 1 D nanostructures with a very restrictive shape, *e.g.* their cross-sections have a rectangular, well faceted appearance. In order to uniquely identify 1 D nanostructures as nanobelts or ribbons, they should be imaged as cross-sections (as the examples shown in Figure 3) or series of images can be taken whilst tilting the nanostructure radially around its long axis. Such an experiment was performed on a SnS_2 nanostructure (identified by EDX analysis within the TEM) liberated from a 80 nm AAM (Figure 8). When the 1 D nanostructure is imaged at tilting angle of 0 degrees its diameter is about 80 nm (Figure 8 (a)); after a radial tilt to 45 degrees the diameter of the nanostructure is reduced to about 60 nm, verifying its nanobelt shape (Figure 8 (b)). Tilting the nanostructure changes the viewing direction hence altering the SAED pattern; thus at a tilting angle of 0 degrees, the SnS_2 nanobelt is imaged along the [211] direction with a SAED pattern (Figure 8 (d)), demonstrating the [011] direction as its growth direction (indexation is done after simulating the SAED pattern, Figure 8 (g)). After altering the tilting angle to 45 degrees the viewing direction is changed to [111] with a corresponding SAED pattern shown on Figure 8 (e), and showing the same growth direction. The upper part of the SnS_2 nanobelt on Figure 8 (c) showed pronounced increase of the nanobelt thickness verified by increased contrast, suggesting

over-lapped nanobelts. The SAED from this part of the image showed a pattern typical for nanocrystal systems having planar defects (Figure 8 (f)), illustrating the case of inter-grown nanobelts (see below for further justification).

The large variety and distinctiveness of the SnS_x nanostructures (nanobelts, nanowires and faceted nanotubes) encouraged us to perform extensive HRTEM analysis of the structures within the channels of the AAMs. Figure 9 presents cross-sections of several different SnS_x nanostructures within 80 nm channels. The most frequently occurring nanostructures are radially inter-grown SnS_2 nanobelts, stacked together to fill the interior of the alumina channels (inset in Figure 9 (a)). Typically these 1 D nanostructures exhibit planar defects such as stacking faults or lengthwise twins along the growth direction. The number of inter-grown nanobelts within a single channel can vary between 2 and 6, thus leading to different filling of the channels. The structure of one of the nanobelts is single crystalline as imaged by the HRTEM (Figure 9(a)) with distinct lattice fringes corresponding to the {001} set of planes (d-spacing of 5.67 nm) grown in a direction parallel to the thickness of the nanobelt and perpendicular to its long axis. In some cases single nanobelts are observed within a channel (inset in Figure 9(b)). HRTEM image of such a nanobelt is shown on Figure 9 (b). The nanobelt is about 10 nm thick with well visible crystalline fringes depicting its single crystalline nature. After performing Fast Fourier transformation (FFT) of the HRTEM image, the accurate lattice dimensions were obtained (inset in Figure 9 (b)). Thus it was determined that the nanobelt has a SnS structure with the {101} set of planes (d-spacing of 0.32 nm) and {020} set of planes (d-spacing of 0.6 nm) that are oriented perpendicular to each other, the latter being parallel to the thickness of the nanobelt. Normally, such single nanobelts within a channel are free of defects and highly crystalline.

A completely different nanostructure is shown on Figure 9 (c), where a highly distorted single nanobelt can be observed. In this case, a SnS_2 nanobelt is formed (identified by the indexation of the FFT), having curled structure and forming half a nanotube. HRTEM imaging evidenced that {001} set of planes, oriented parallel to the thickness of the nanobelt, were under high stress, forming dislocation defects in order to accommodate the curvature of the alumina wall (the distortion of the lattice planes is

shown with arrows). Instead of forming multi-layered, inter-grown nanobelts within a single channel, the growth process probably proceeds along the {001} set of planes, eventually exceeding the diameter of the alumina channel, and the crystal structure is bent to follow the curvature of the pore wall.

Another example of the alumina channels confining the growth and thus influencing the shape of the nanostructures is exemplified in Figure 9 (d). Here the distortion of the nanobelt structure resulted in the formation of a plane defect, *e.g.* the formation of a twinned structure. The twining boundary is easily recognizable. The right segment of the twin has a SnS_2 structure and is imaged along the [100] zone axis as evidenced by the FFT of the HRTEM image (inset in Figure 9 (d)). Here the {001} set of planes are parallel to the thickness of the segment, while the most pronounced lattice fringes (shown with bars) are of the {012} set of planes having d-spacing of 0.22 nm and oriented at 130 degrees to the {001} set of planes. Apparently the twining system is (012)[001] with the twining elements given in Figure 9 (d). More importantly the alumina walls play crucial roles in the formation of this type of nanostructure. Since twining is not very common in SnS_x nanostructures, nor it was observed for material deposited on the outer surface of the membrane, twining is probably a result of the confined environment. Following the curvature of the alumina channel, twinned SnS_x crystals are grown on the alumina surface, thus forming faceted nanotubes or half-tubes (see before SEM images for more examples of faceted nanotubes). Similar investigations were performed with the SnS_x nanostructures deposited within 20 nm channels (see Supporting Information). Generally, less defective nanostructures were observed, predominantly in the shape of nanobelts and nanowires.

Crystal structure and growth within confined environments

With the aim of elucidating possible confinement affects on the growth process, the crystal structure and morphology of the materials grown on the surface of the membranes was compared to that deposited within the channels.

For example, 1 D structures of Bi_2S_3, with variable lengths and diameters, some of them exceeding several micrometers (Figure 10 (a)), were grown on the surface of the AAMs. . This type of morphology is not surprising since it is known that Bi_2S_3 is a layered material, wherein the layers are connected *via*

weaker intermolecular Bi – S bonds. This is a unique feature of the material that can give rise to potential nanostructures under certain conditions. Thus exfoliation of the crystal structure along the weak intermolecular bonds, or the rapid growth of the crystal along the *c*-axis may give rise to dimensional structures such as nanosheets or nanofibers.[6b] Therefore it is not surprising that the 1 D growth of the encapsulated nanostructures is along the *c*-axis (seen by SAED, HRTEM and XRD), and results in highly oriented single crystalline nanowires. Therefore, the role of the channels within the templates is to entrap and vertically guide the growth of the Bi_2S_3 material, thus restricting the formation of larger diameter nanostructures but not excluding the formation of smaller diameter nanowires (some of them seen in a single channel).

A completely different type of morphology was observed for the CdS material deposited on the outer membrane surface (Figure 10 (b)). The membrane surface was fully covered with a continuous layer of CdS with no particular shape of crystallites. Conversely, the embedded CdS material showed well define nanowire morphologies with pronounced single crystalline and oriented nature. Therefore the role of the channels within the templates is not only to entrap the deposited material but also to form the shape of the 1 D nanostructures. Slightly distorted single crystalline nanostructures of CdS, due to strain as seen by SAED, result from the influence of the alumina channels. Similarly to the Bi_2S_3 samples, the nanostructures are grown along the *c*-axis (seen by SAED, HRTEM and XRD) which is known to be the fastest growth rate direction when dimensional CdS nanocrystals are formed.[6g]

From the crystallographic point of view, the most interesting structures are those of SnS_x deposited within the AAMs. Due to the versatile coordinating characteristics of tin and sulphur, tin sulfide shows a variety of phases, such as SnS, SnS_2, Sn_2S_3, and Sn_3S_4. Based on the SAED, EDX and XRD data only two phases, *e.g.* SnS and SnS_2 were identified as nanostructures deposited within the AAMs. By comparison, the material grown on the membrane surface is of single phase SnS in the form of micro-sized sheets (Figure 9 (c)). This is not surprising since SnS belongs to the group of layered semiconductors with two SnS layers in a unit cell where one of the long distance S atoms actually resides on the neighbouring SnS layer (Figure 9 (d)). This weak Sn-S interaction binds the two tin

sulfide layers together to form a double layer structure. Possible exfoliation of the crystal structure along the weak intermolecular bonds, or the rapid growth of the crystal along the *c*-axis may give rise to dimensional structures such as sheets or fibres. Within the confined environment of the alumina pores, growth of SnS is restricted along the *a*- or *b*-axis resulting in the formation of well faceted nanobelts (Figure 9 (d)). The SnS layers extend along the *c*-axis with the {002} set of planes parallel to the long axis of the 1 D nanostructures (seen by SAED and XRD)

Similarly SnS_2 has a lamellar structure in which the tin atoms are located in octahedral interstices between two hexagonally close packed sulphur slabs to form a three-atom layered sandwich structure. The SnS_2 layers are then stacked on top of one other along the crystallographic *c*-axis and held together by weak van der Waals forces (Figure 10 (d)). There are many ways to stack these layers together to create various polytypes. More than 70 polytype structures of SnS_2 have been identified. All the polytypes have an identical unit cell parameter $a = 0.365$ nm; however they exhibit a different parameter *c* orthogonal to the layer which is an integral number of the inter-lamellar spacing of 0.589 nm. The thermodynamically stable polytype of SnS_2 (berndtite) at ambient conditions consists of a trigonal lattice *P3m* ($a = 0.364$ nm; $c = 0.589$ nm) with one layer as a repeat unit. When such structures are formed within a confined environment, the stacking of the SnS_2 layers in the direction parallel to the *c*-axis is restricted resulting in the formation of nanobelts or stacks of inter-grown nanobelts. The growth of the SnS_2 layers can also be constrained in the *a*-*b* plane leading to considerable deformation of the uniformity of the SnS_2 layers (Figure 10 (d)). This restriction results in bending of the SnS_2 sheets and the formation of defective nanostructures such as curled or faceted nanotubes or half-tubes (seen by SEM, HRTEM and SAED).

Generally, the growth process for the deposition of the sulfide nanostructures discussed in this paper can be described as one starting from a precursor melt, pre-loaded inside the channel of the templates, and is ruled by the intrinsic crystalline structure of the encapsulated materials in conjunction with the highly anisotropic nature of the alumina matrix. The incorporation of the melted precursors, without use of additional solvents, within the alumina channels is regulated by the capillary forces and is dependent

on the surface tension (wet-ability of the alumina walls), viscosity of the precursors melt and diameter of the channels. After decomposition of the single source precursors and when the supersaturation is reached at the desired temperature, the crystallisation process starts leading to the formation of the final crystalline structures. This crystallisation process results in volume contraction leading to free voids for additional mass transfer of precursor. Evidences supporting that mechanism are the existence of inter-grown nanobelt stacks in the case of SnS_x samples and the formation of smaller diameter nanowires in the case of the Bi_2S_3 material. Apparently, this process is limited by the efficiency of the mass transfer being completely hindered when the alumina channels are blocked. These restrictions together with the limitations resulting from inefficient loading of the alumina channels with melted precursors are the most important reasons for the non-uniform loading of nanostructures across the membrane thickness, as seen observed by cross-sectional EDX analysis. Nevertheless, even with a pore filling factor of 60 % (mean value for the three sulfides), the densities of the nanostructures within the 80 and 20 nm membranes are: 1×10^9 and 6×10^9 per cm^2, respectively.

Conclusions

Using electron microscopy and spectroscopy we were able to comprehensively investigate the growth process and structure of 1 D Bi_2S_3, CdS and SnS_x nanostructures within the channels of the AAMs. Important characteristics such as morphology, loading factors, crystal structure, orientation and possible growth mechanisms within the confining environments of 80 and 20 nm alumina channels were discussed. It has been shown that by combining a solventless pressure-injection method and AAMs as hard templates, ordered arrays of 1 D nanostructures with controlled diameters (by the dimensions of the templating channels), controlled orientations (by the orientation of the templating channels) and isolated from each other within an alumina matrix can be formed. A variety of 1 D nanostructures ranging from well faceted nanowires to nanotubes and nanobelts have been identified and characterized by HRTEM, SAED and EDX. For all of the metal sulfides studied, single crystalline and oriented structures were observed having preferred growth directions within the AAMs channels. Integration of such structures into useful architectures may be useful for creation of functional nanosized devices.

ACKNOWLEDGMENT The authors thank Science Foundation Ireland (Grant No.: 03/IN3/I375) for the financial support.

SUPPORTING INFORMATION PARAGRAPH **Supporting Information Available**. Additional plan-view TEM images of the encapsulated 1 D nanostructures are presented.

FIGURE CAPTIONS

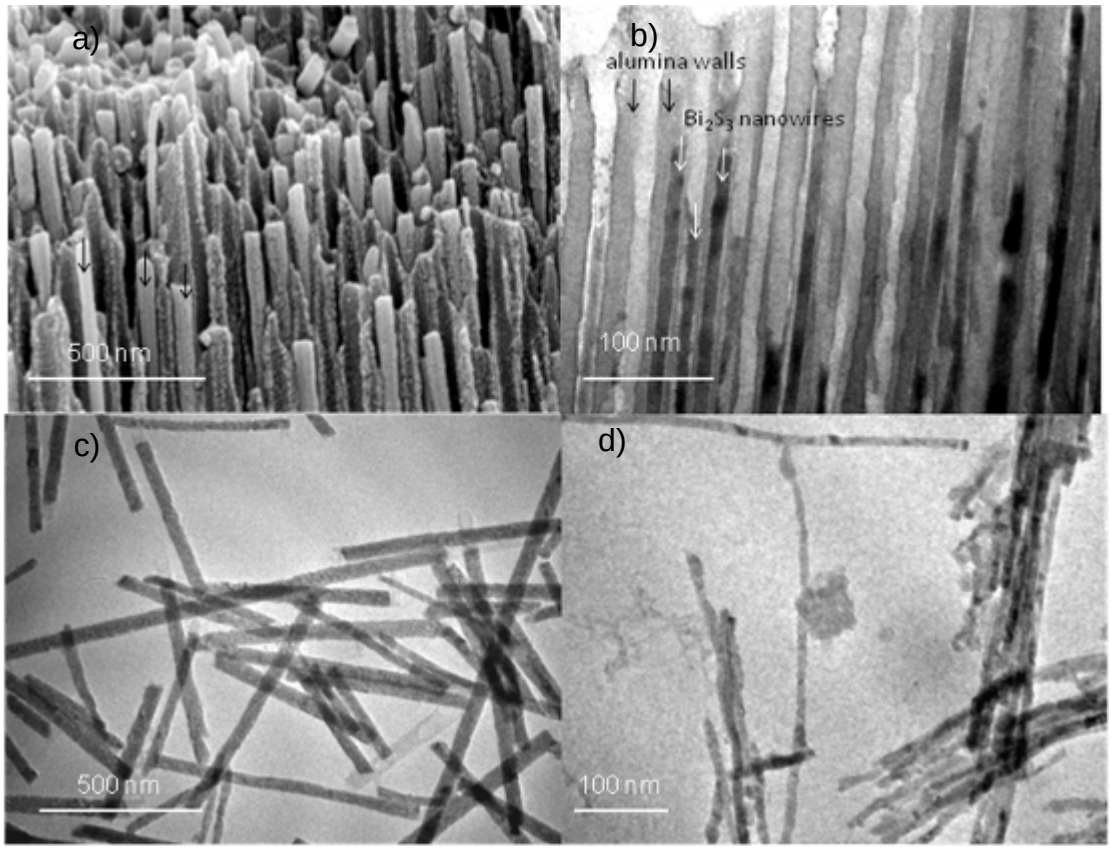


Figure 1. Cross-section SEM and TEM images of Bi_2S_3 nanowires within 80 and 20 nm AAMs (a) and (b), and TEM images of isolated CdS nanowires from 80 and 20 nm AAMs (c) and (d).

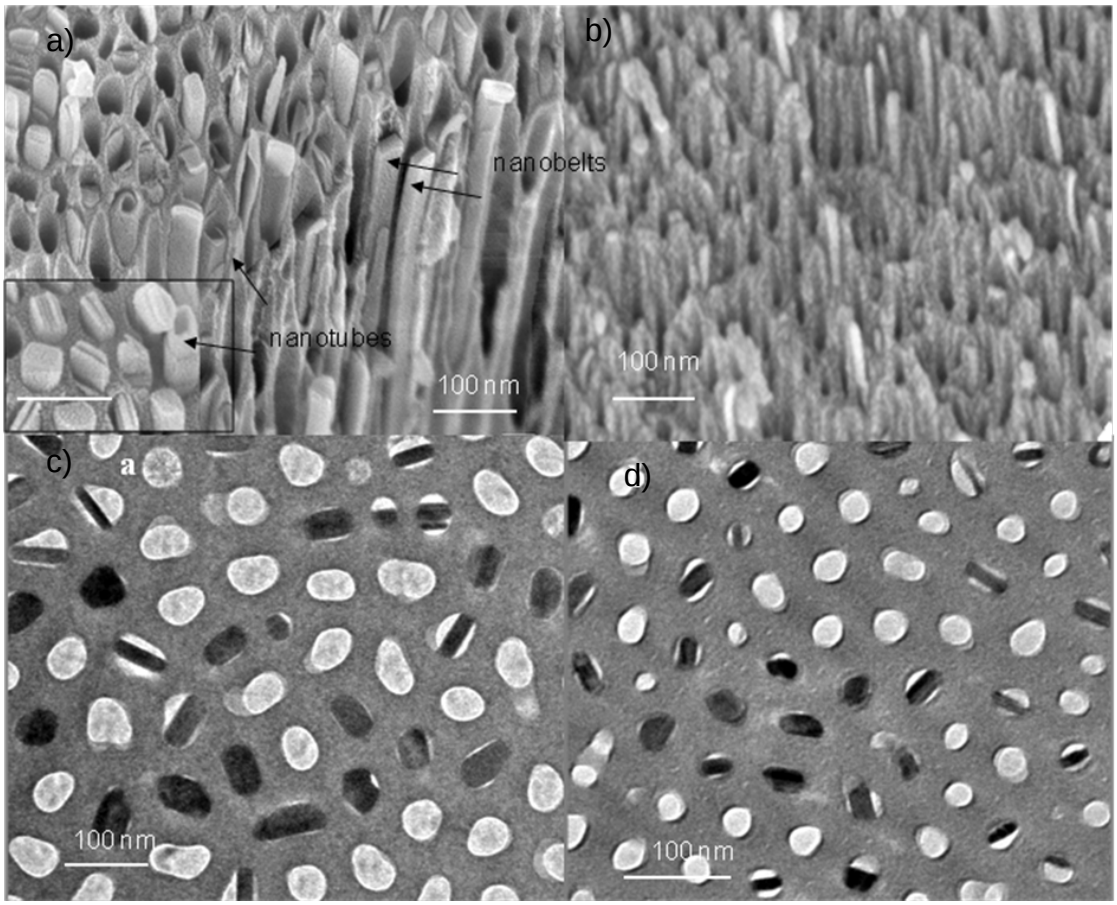


Figure 2. Cross-section SEM images of the SnS_x nanostructures within 80 and 20 nm AAMs (a) and (b), and the corresponding plan-view TEM images (c) and (d).

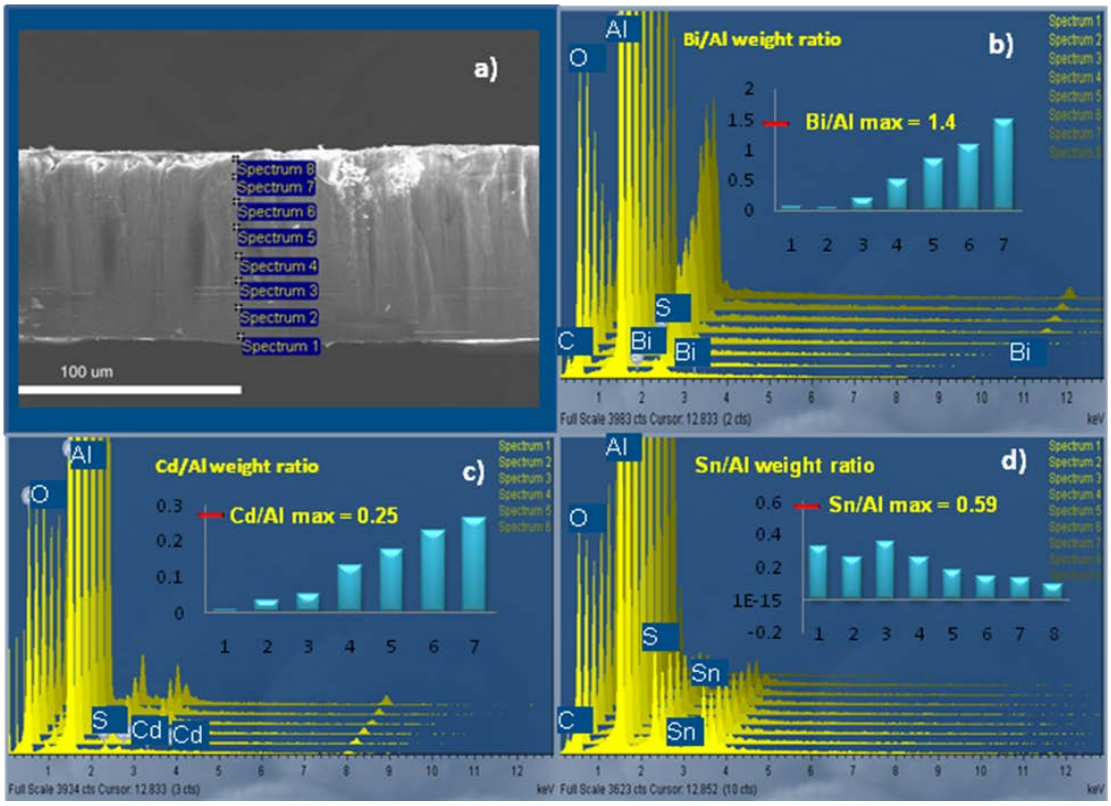


Figure 3. Cross-section SEM image of the 80 nm AAM with the positions where EDX spectra were taken (a) and the EDX spectra for the Bi_2S_3 (b), CdS (c) and SnS_x (d) samples (insets: corresponding Me/Al weight ratios and calculated Me/Al ratios at maximum loading).

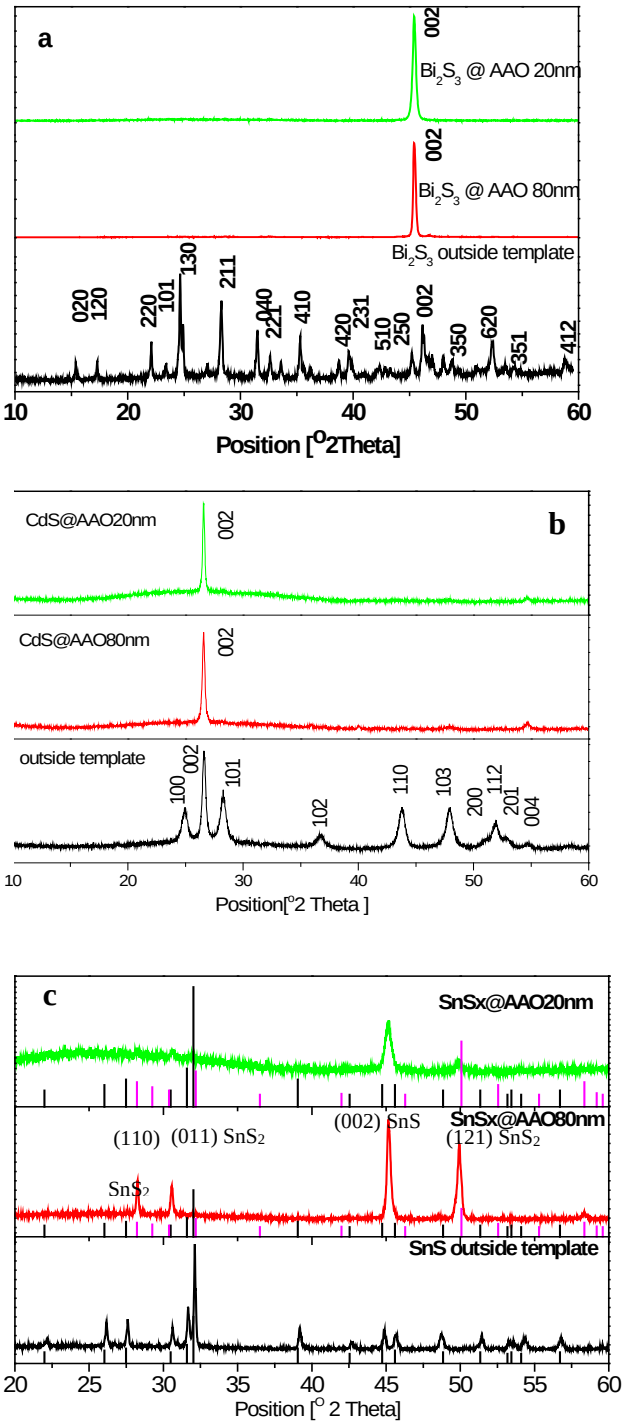


Figure 4. XRD patterns of membranes with material deposited outside the template (black), within 80 nm AAMs (red) and within 20 nm AAMs (green) for the Bi2S3 (a), CdS (b) and SnSx (c) samples.

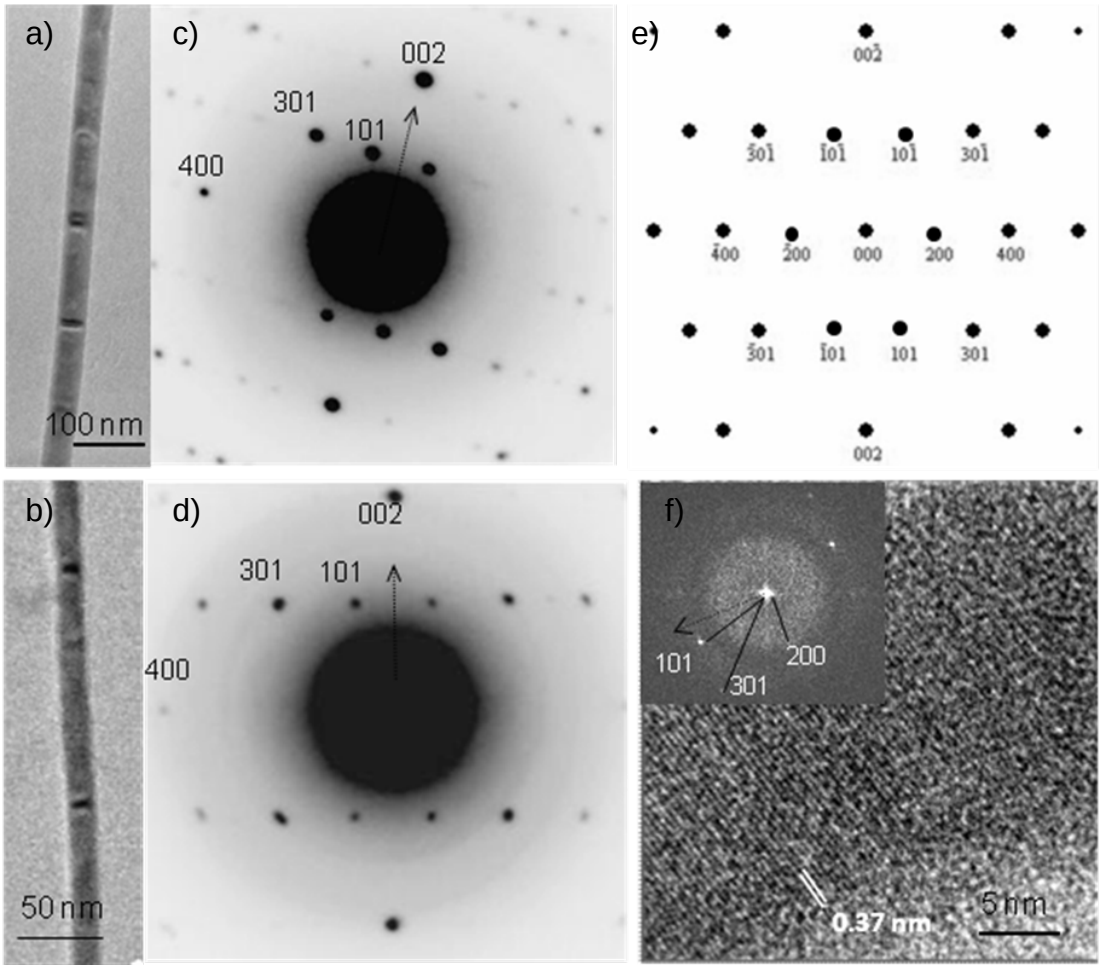


Figure 5. TEM images of 80 and 20 nm Bi_2S_3 nanowires (a) and (b), with the corresponding SAED patterns (c) and (d), simulated ED pattern with the electron bean along the [010] zone axis (e) and HRTEM image of a 20 nm Bi_2S_3 nanowire (inset corresponding FFT of the image) (f). Growth directions are shown with arrows.

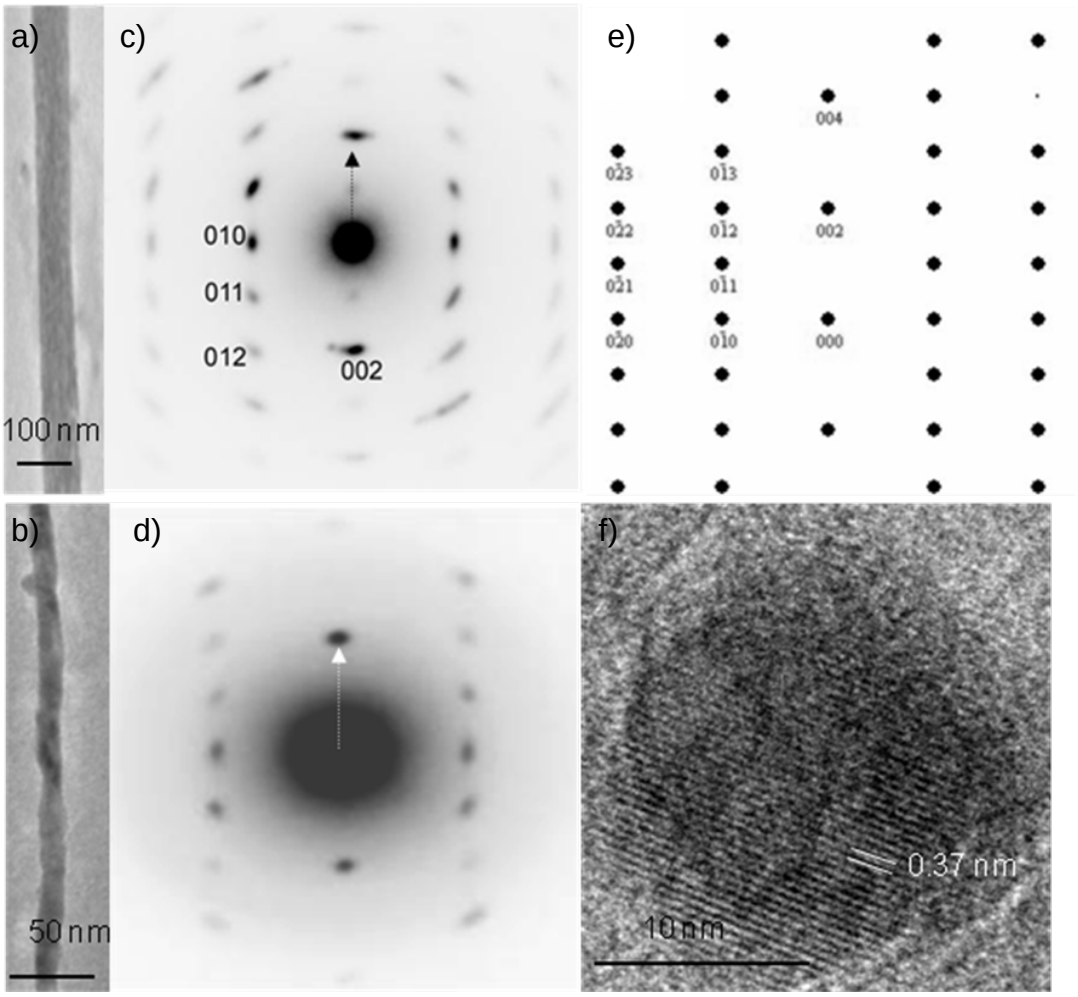


Figure 6. TEM images of CdS nanowires grown with 80 and 20 nm AAMs (a) and (b), with the corresponding SAED patterns (c) and (d), simulated ED pattern with the electron bean along the [100] zone axis (e) and HRTEM image of a CdS nanowire grown within the single channel of a 20 nm AAM (f). Growth directions are shown with arrows.

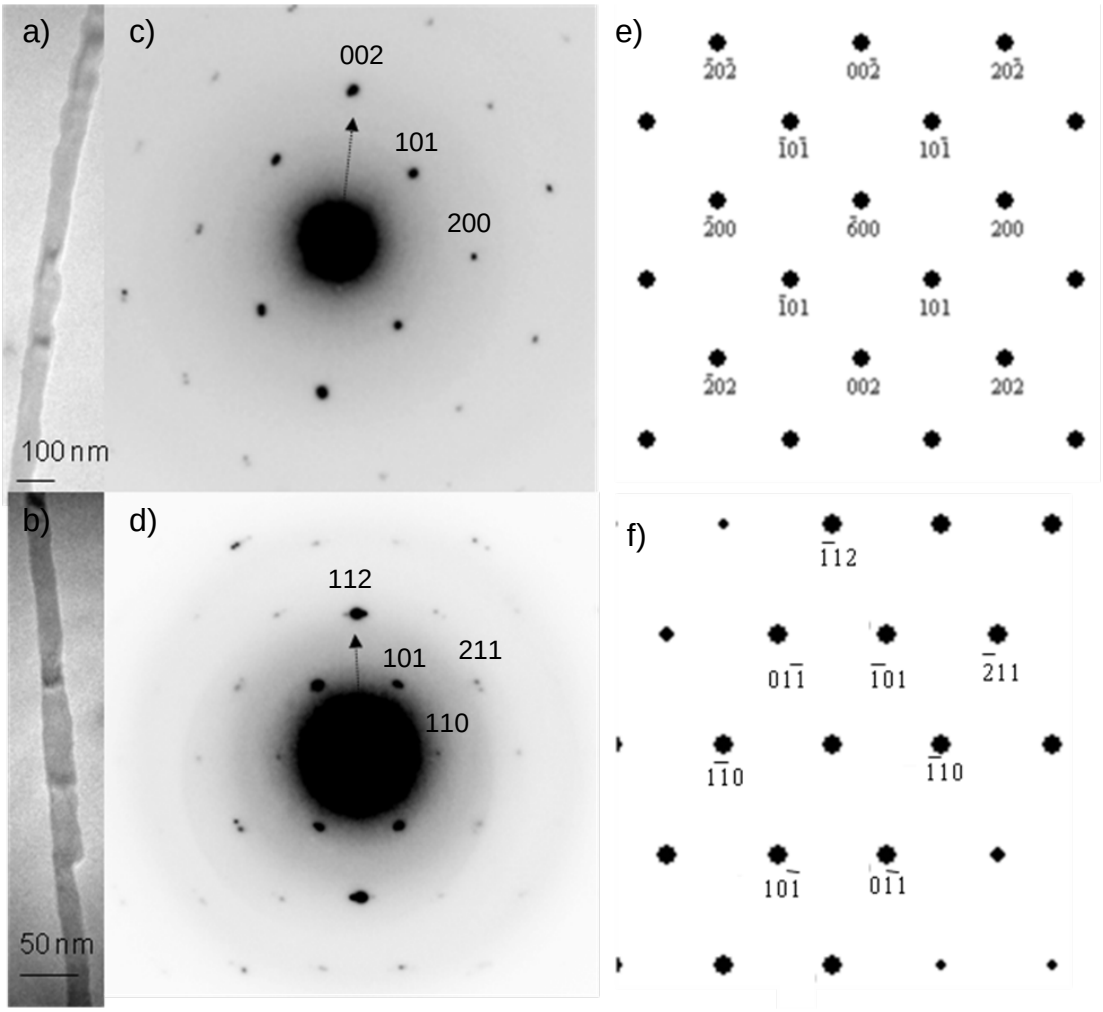


Figure 7. TEM images of 80 nm SnS (a) and b SnS_2 nanobelts (b), with the corresponding SAED patterns (c) and (d), and simulated ED pattern for the SnS phase with the electron bean along the [010] zone axis (e), and for the SnS_2 phase with the electron beam along the [111] zone axis (f). Growth directions are shown with arrows.

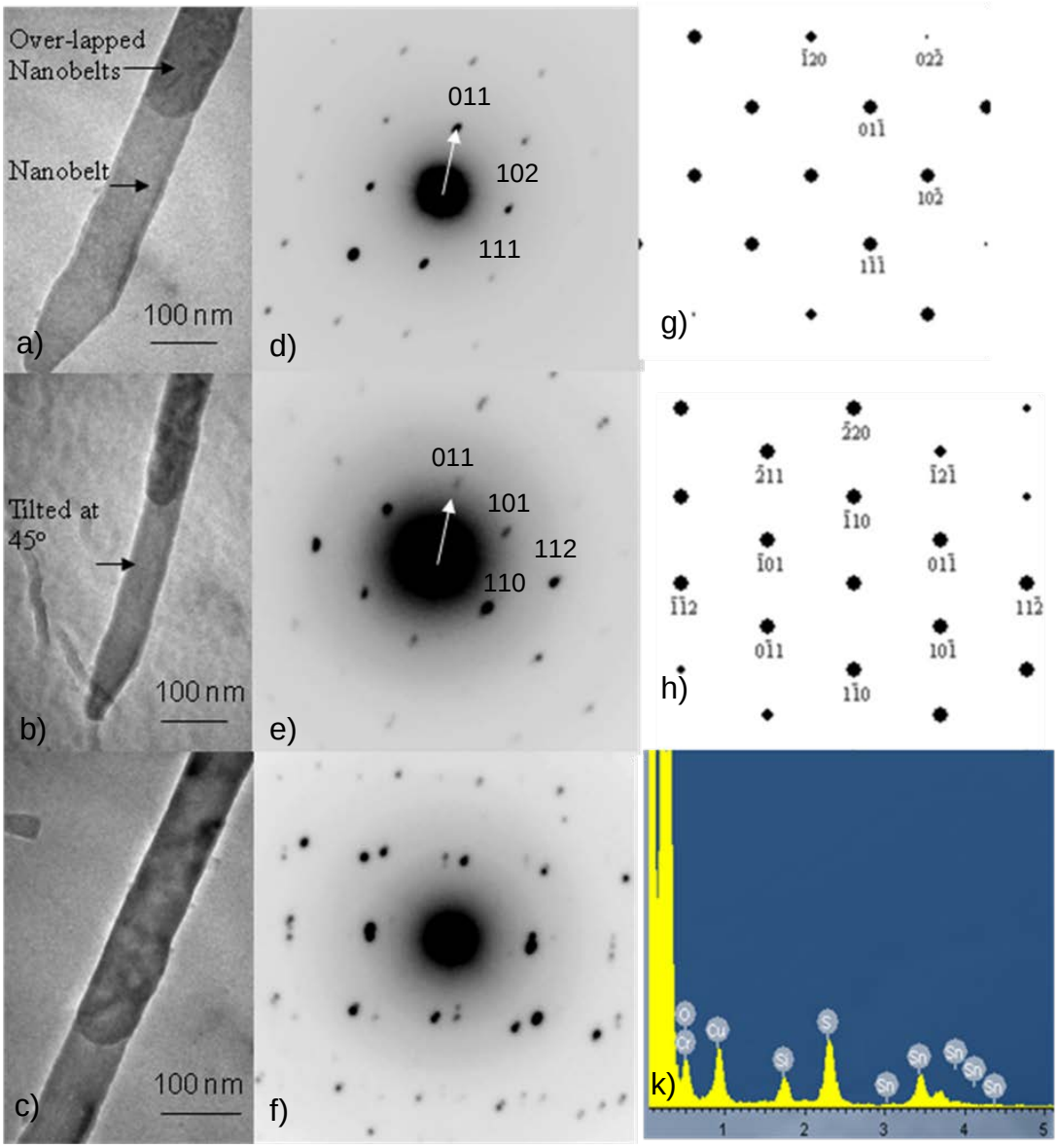


Figure 8. TEM images of a SnS_2 nanobelt grown within an 80 nm AAM at different radial tilting angles of (a) 0° and (b) 45° and in the region where the nanobelts are over-lapped (c), with the corresponding SAED patterns (d), (e) and (f), simulated ED patterns for the SnS_2 phase with the electron bean along the [211] zone axis (g) and along the [111] zone axis (h), and corresponding EDX spectrum (k). Growth directions are shown with white arrows.

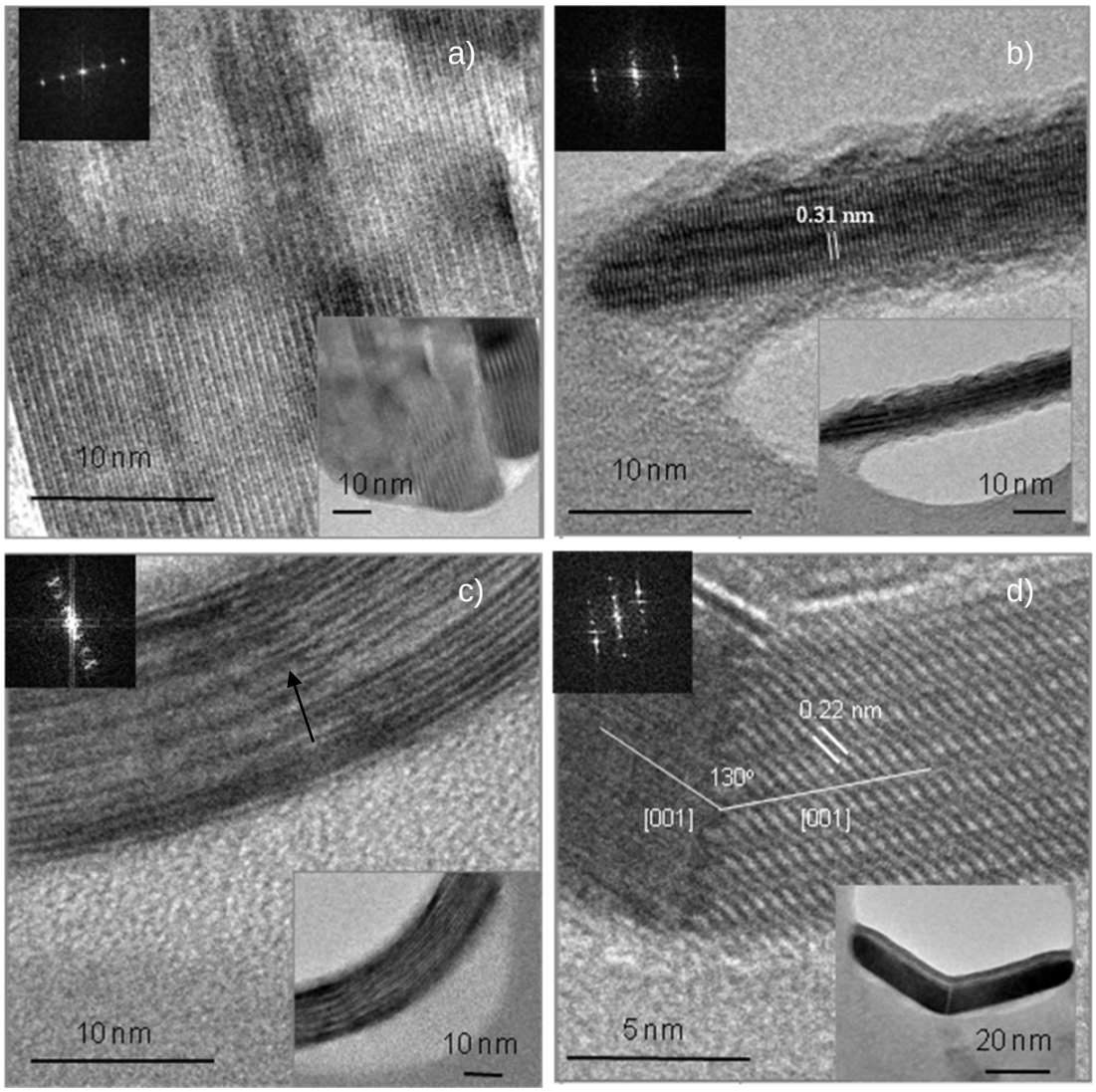


Figure 9. HRTEM images of cross-sections of different SnS_x nanostructures encapsulated within AAMs channels showing stacked nanobelts (a), single nanobelt (b), bent nanobelt and twined nanobelt (d) (insets: corresponding FFTs).

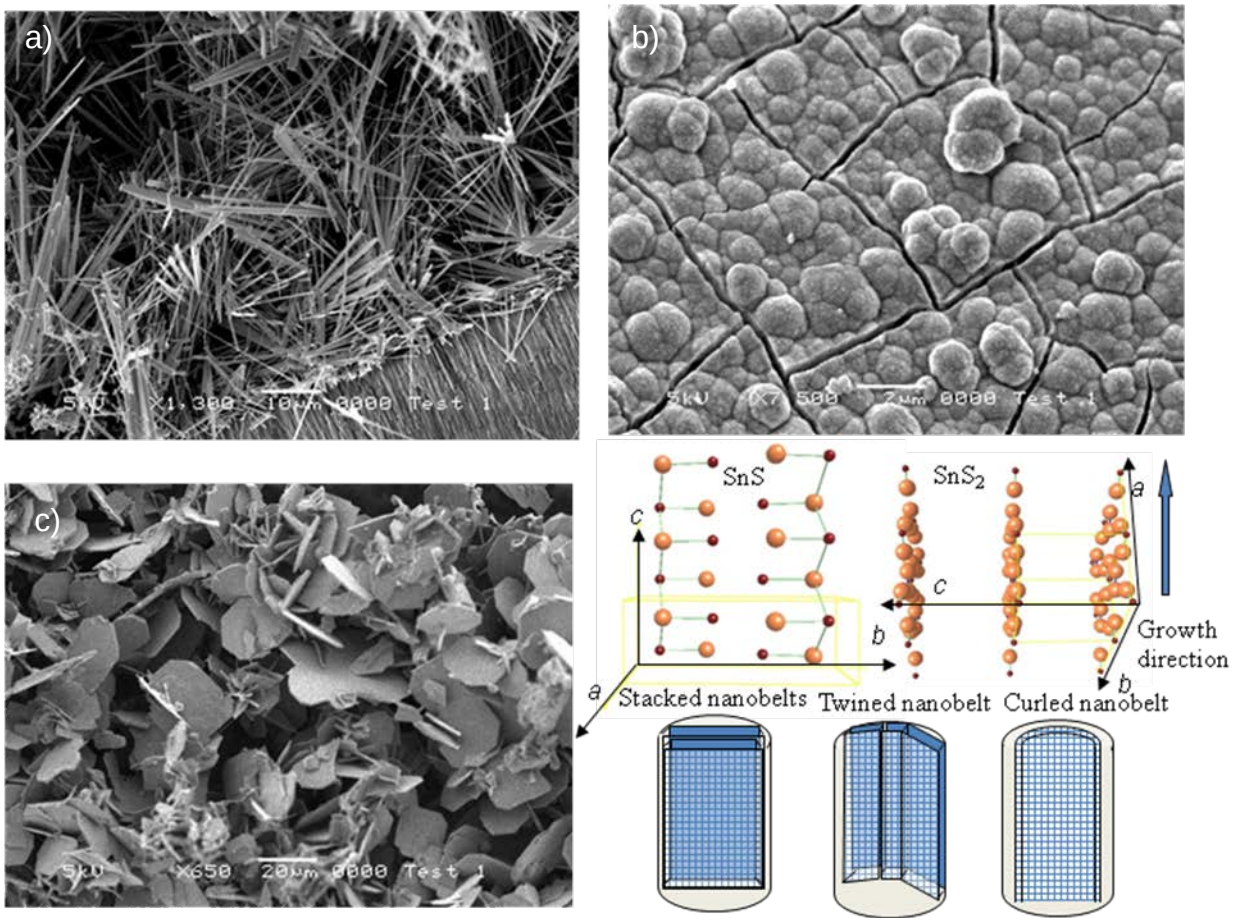


Figure 10. SEM images of the material deposited on the outer surface of the AAMs for the Bi_2S_3 (a), CdS (b) and SnS_x (c) samples, and schematics of the crystal structures and morphologies of the SnS_x nanostructures within AAMs.

REFERENCES

(1) For example, see the following reviews and the references therein: (a) Thelander, C.; Agarwal, P.; Brongersma, S.; Eymery, J.; Feiner, L. F.; Forchel, A.; Scheffler, M.; Reiss, W.; Ohlsson, B. J.; Goesele, U.; Samuelson, L. *Materials Today*, **2006**, 9, 28; (b) Lieber C. M.; and Wang, Z. L. *MRS Bulletin*, **2007**, 32, 99; (c) Fan, H. J.; Werner, P.; Zacharias, M. *Small*, **2006**, 2, 700.

(2) (a) Foss, C. A.; Tierney, M. J.; Martin, C. R. *J. Phys. Chem.* **1992**, 96, 9001; (b) Preston, C. K. and Moskovits, M., *J. Phys. Chem.* **1993**, 97, 8495; (c) Whitney, T. M.; Jiang, J. S.; Searson, P. C.; Chien, C. L. *Science*, **1993**, 261, 1316; (d) Martin, B. J.; Dermody, D. J.; Reiss, B. D.; Fang, M.; Lyon, A.; Nata, M. J.; Mallouk, T. E. *Adv. Mater*. **1999**, 11, 1021.

(3) (a) Lakshmi, B. B.; Dorhot, P. K.; Martin, C. R. *Chem. Mater*. **1997**, 9, 857; (b) Suh, J. S.; Lee, J. S. *Appl. Phys. Lett.* **1999**, 75, 2047; (c) Tian, M.; Wang, J.; Kurtz, J.; Mallouk, T. E.; Chan, M. H. W. *Nano Lett.* **2003**, 3, 919; (d) Lee, W.; Scholz, R.; Nielsch, K.; Goesele, U. *Angew. Chem. Int. Ed.* **2005**, 44, 6030; (e) Bogart, T. E.; Dey, S.; Lew, K-K.; Mohney, S. E.; Redwing, J. M. *Adv. Mater.* **2005**, 17, 114; (f) Cott, D. J.; Petkov, N.; Morris, M. A.; Platschek, B.; Bein, T.; Holmes, J. D. *J. Am. Chem. Soc.* **2006**, 128, 3920; (g) Petkov, N.; Platschek, B.; Morris, M. A.; Holmes, J. D.; Bein, T. *Chem. Mater.* **2007**, 19, 1376.

(4) (a) Lahav, M.; Sehayek, T.; Vaskevich, A.; Rubinstein, I. *Angew. Chem. Int. Ed.* **2003**, 47, 5576; (b) Wang. J.; Tian, M.; Mallouk, T. E.; Chan, M. H. W. *J. Phys. Chem. B* **2004**, 108, 841; (c) Liang, Y.; Zhen, C.; Zou, D.; Xu, D. *J. Am. Chem. Soc.* **2004**, 126, 16338; (d) Petkov, N.; Pavels Birjukovs, P.; Phelan, R.; Morris, M. A.; Erts D.; and Holmes J. D. *in press.*

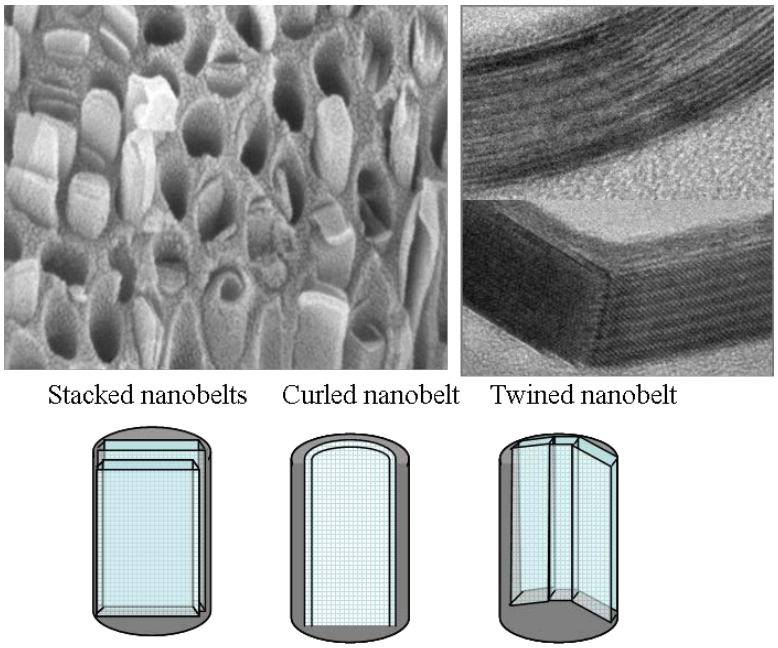
(5) Xu, J.; Petkov, N.; Wu, X.; Iacopino, D.; Quinn, A. J.; Redmond, G.; Bein, T.; Morris, M. A.; Holmes, J. D, *ChemPhysChem* **2007**, 8, 235.

(6) (a) Yu, Y.; Jin, C. H.; Wang, R. H.; Chen, Q.; Peng, L.-M. *J. Phys. Chem. B* **2005**, 109, 18772; (b) Sigman, M. B. Jr. and Korgel, B. A. *Chem. Mater.* **2005**, 17, 1655; (c) Jiang, T and Ozin, G. A. *J. Mater. Chem.* **1998**, 8, 1099; (d) Hong S. Y.; Popovitz-Biro, R.; Prior, Y.; Tenne, R.; *J. Am. Chem. Soc.* **2003**, 125, 10470; (e) Xu, D.;. Xu. Y.; Chen, D.; Guo, G.; Gui, L.; Tang, Y. *Adv. Mater.* **2000**, 12, 520; (f) Li, Y.; Xu, D.; Zhang, Q.; Chen, D.; Huang, F.; Xu, Y.;. Guo, G.; Gu, Z. *Chem. Mater.* **1999**, 11, 3434; (g) Shieh, F.; Saunders, A. S.; Korgel, B. A. *J. Phys. Chem. B* **2005**, 109, 8538.

(7) (a) Xia, Y.; Yang, P.; Sun, Y.; Wu, Y.; Mayers, B.; Gates, B.; Yin, Y.; Kim, F.; Yan, H.; *Adv. Mater*. **2003**, 15, 353; (b) Dresselhaus, M. S.; Lin, Y. M.; Rabin, O.; Jorion, A.; Souza Filho, A. G.; Pimenta, M. A.; Saito, R.; Samsonidze, G. G.; Dresselhaus, G. *Mater. Sci. Eng. C* **2003**, 23, 129.

(8) (a) Bell, D. C.; Wu, Y.; Barrelet, C. J.; Gradecak, S.; Xiang, Jie.; Timko, B. P.; Lieber, C. M. *Micro. Res. Tech.* **2004**, 64, 373; (b) Ding, Y. and Wang, L. *J. Phys. Chem. B* **2004**, 108, 12280; (c) Wang. Z. L. *Adv. Mater*. **2000**, 12, 1296.

TOC Figure



Using electron microscopy and spectroscopy we were able to comprehensively investigate the growth process and structure of 1 D Bi_2S_3, CdS and SnS_x nanostructures within the channels of the anodic alumina membranes (AAMs). A variety of 1 D nanostructures ranging from well faceted nanowires to nanotubes and nanobelts have been identified, having single crystalline and oriented structure within the AAMs.